TISSUE ENGINEERING: Part C
Volume 23, Number 8, 2017

DOI: 10.1089/ten.tec.2017.0133

termis
Tissue Engineering
& Regenerative Medicine
International Society

METHODS ARTICLE

Human Induced Pluripotent Stem Cell-Derived Endothelial Cells for Three-Dimensional Microphysiological Systems

Yosuke K. Kurokawa, BS,[1] Rose T. Yin, BS,[1] Michael R. Shang, BS,[1] Venktesh S. Shirure, PhD,[1] Monica L. Moya, PhD,[2] and Steven C. George, MD, PhD[1,3]

Microphysiological systems (MPS), or ''organ-on-a-chip'' platforms, aim to recapitulate *in vivo* physiology using small-scale *in vitro* tissue models of human physiology. While significant efforts have been made to create vascularized tissues, most reports utilize primary endothelial cells that hinder reproducibility. In this study, we report the use of human induced pluripotent stem cell-derived endothelial cells (iPS-ECs) in developing three-dimensional (3D) microvascular networks. We established a *CDH5*-mCherry reporter iPS cell line, which expresses the vascular endothelial (VE)-cadherin fused to mCherry. The iPS-ECs demonstrate physiological functions characteristic of primary endothelial cells in a series of *in vitro* assays, including permeability, response to shear stress, and the expression of endothelial markers (CD31, von Willibrand factor, and endothelial nitric oxide synthase). The iPS-ECs form stable, perfusable microvessels over the course of 14 days when cultured within 3D microfluidic devices. We also demonstrate that inhibition of TGF-β signaling improves vascular network formation by the iPS-ECs. We conclude that iPS-ECs can be a source of endothelial cells in MPS providing opportunities for human disease modeling and improving the reproducibility of 3D vascular networks.

Keywords: endothelial cells, induced pluripotent stem cells, microfluidics, vascularization

Introduction

Nearly every tissue within the human body relies on vasculature for delivery of nutrients and oxygen and removal of waste. In addition, the endothelial cells (ECs) that line the vasculature play critical roles in organ development, homeostasis, and disease progression.[1–3] The burgeoning field of microphysiological systems (MPS, or ''organ-on-a-chip'') seeks to create human tissue mimics at the micron to millimeter scale. These model systems have important applications in the areas of *in vitro* pharmacokinetic modeling, drug toxicity, and drug efficacy. The incorporation of dynamic and functional vascular networks into MPS remains a priority, as it significantly advances the physiological relevance of these systems.[4–7] A variety of methods have been developed for creating three-dimensional (3D) vasculature *in vitro*,[8–10] but we and others have focused on utilizing the native vasculogenic program of endothelial cells to spontaneously form robust and perfusable vascular networks in microfluidic devices.[11–18] Such methods are amenable to including other functional cells types (e.g., hepatocytes, cardiomyocytes) to create complex, vascularized tissues that may be used for drug screening and mechanistic studies.[19–22]

While efforts in the field have mostly revolved around the use of primary cells, there has been growing interest in using human pluripotent stem cells (hPSCs) as the source of endothelial cells to create vessel networks. Employing a single stem cell line to derive endothelial cells has several important advantages. First, concerns over donor-to-donor variability in primary cells are ameliorated. Second, advances in gene editing (e.g., clustered regularly interspaced short palindromic repeats) have facilitated the creation of stem cell lines that have useful reporters or modified functions for mechanistic studies.[23] Finally, the use of human induced pluripotent stem cells (hiPSCs) offers the potential to perform disease-specific and patient-specific drug screening *in vitro*.[7,24–27] Future

[1]Department of Biomedical Engineering, Washington University in St. Louis, St. Louis, Missouri.
[2]Center for Micro and Nano Technology, Materials Engineering Division, Lawrence Livermore National Laboratory, Livermore, California.
[3]Department of Energy, Environment, and Chemical Engineering, Washington University in St. Louis, St. Louis, Missouri.

applications may also include using iPSC-derived endothelial cells (iPS-ECs) as an autologous cell source for regenerative medicine.

Several differentiation protocols now exist to create endothelial cells from hPSCs, usually defined by the expression of definitive endothelial markers such as platelet-endothelial cell adhesion molecule-1 (PECAM1, or CD31), vascular endothelial (VE)-cadherin (CD144), endothelial nitric oxide synthase (eNOS), and von Willebrand factor (vWF).[28–30] However, studies that investigate their potential uses in MPS have been limited. Belair *et al.*[18] recently showed promising results using iPS-ECs for various *in vitro* assays that demonstrate their physiological functions. In particular, they demonstrate the key roles of VEGF and FGF signaling in sprouting angiogenesis of iPS-ECs. Most previous works have used primary cell sources such as human umbilical vein endothelial cells (HUVECs) and endothelial colony-forming cell-derived endothelial cells (ECFC-ECs), with ECFC-ECs being considered the desired cell source due to their high proliferative capacity and vasculogenic potential.[31] It is of great interest in the field to further understand how iPS-ECs perform in these platforms, thus providing an important alternative to primary endothelial cells.

Herein, we investigate the vasculogenic potential of iPS-ECs derived from an mCherry-VE-Cadherin fusion protein reporter iPSC line. The cells demonstrate physiological functions of endothelial cells, display a predominantly venous phenotype, respond to shear stress, and form perfusable vascular networks within 3D microfluidic devices. We also demonstrate drug screening capabilities of the platform by observing changes in the vasculature in response to small molecule inhibitors.

Materials and Methods

Cell culture

Two human iPSC lines were used in the experiments: WTC11 (gifted by Dr. Bruce Conklin, Gladstone Institutes) and C2A (gifted by Dr. Gordana Vunjak-Novakovic, Columbia University). The iPSCs were cultured as described previously,[32] with modifications. Briefly, the cells were grown on six-well plates coated with growth factor reduced Matrigel (Corning) in Essential 8 (E8) medium (Thermo Scientific) with daily media replacement. The cells were passaged at 80% confluence using StemPro Accutase (Life Technologies) and seeded on Matrigel-coated plates in the E8 medium containing 10 μM Y-27632 (LC Laboratories). All cells were cultured at 37°C and 5% CO_2.

Human umbilical arterial endothelial cells (HUAECs), HUVECs, and human dermal lymphatic endothelial cells (HDLECs) were purchased from PromoCell and cultured according to manufacturer's protocols. ECFC-ECs were isolated and cultured as described previously.[11] Normal human lung fibroblasts (NHLF) were purchased from Lonza and cultured according to manufacturer's protocols. The cells were used between passages 3 and 7.

CDH5-*mCherry iPSC line*

The *CDH5*-mCherry-tagged cell line was generated from the GCaMP6-WTC11 human iPSC line[33] by the Genome Engineering and iPSC Center (GEiC), Washington University in St. Louis. The GCaMP6-WTC11 line constitutively expresses GCaMP6 and can thus be used to report changes in intracellular calcium. Approximately, 2×10^6 WTC11 iPSCs were resuspended in P3 primary buffer and electroporated using a 4D-Nucleofector (Lonza) with 1.5 μg of *CDH5-mCherry* donor plasmid (GeneArt), 1 μg guide RNA (gRNA; MS232.*CDH5*.g11 targets 5′-taggcggccgaggtcactc tgg-3′ near the *CDH5* stop codon) and 1.5 μg Cas9 vectors using nucleofection program CA-137. Following nucleofection, cells were single-cell sorted and screened with polymerase chain reactions (PCRs) using primer sets specific to genomic and donor plasmid regions. The overall nucleofection efficiency was 50–60% based on the expression of a codelivered GFP construct. *CDH5*-mCherry-tagged region of final clones was sequence confirmed using Sanger sequencing.

Derivation and isolation of iPS-ECs

The iPS-ECs were differentiated following a previously established protocol (Fig. 1A).[34] Briefly, ~80% confluent iPSCs were split 1:4 onto Matrigel-coated tissue culture flasks as described above (day 0). Between days 0 and 2 of differentiation, the cells were cultured in the E8BA medium, which consisted of E8 medium supplemented with 5 ng/mL BMP4 (R&D) and 25 ng/mL Activin A (PeproTech), with daily medium replacement. On day 0 of differentiation, 10 μM Y-27632 was added to the E8BA medium. Between days 2 and 6 of differentiation, the cells were cultured in the E7BVi medium, which consisted of Essential 6 (E6) medium supplemented with 100 ng/mL FGF2 (PeproTech), 10 ng/mL BMP4, 50 ng/mL VEGF-A (PeproTech), and 5 μM TGF-β inhibitor SB431542 (STEMCELL Technologies), with daily medium replacement. On day 6, the cells were passaged using TrypLE (Life Technologies) and sorted using the CD31 Microbead Kit (Miltenyi Biotec) and EasySep™ Magnet (STEMCELL Technologies) following manufacturer's protocols. After purification, the $CD31^+$ cells were cultured on tissue culture flasks coated with human fibronectin (1 μg/cm^2; Millipore) in the E7V medium (E6 + 100 ng/mL FGF2 + 50 ng/mL VEGF-A). The cells were passaged on day 8 using TrypLE and frozen in CryoStor10 (STEMCELL Technologies) at 1×10^6 cells/mL. All experiments were performed using cells between days 10 and 18 differentiation.

Quantitative real-time PCR

RNA was isolated using the RNeasy Plus Mini kit (QIAGEN) following manufacturer's protocols. RNA concentration was measured using NanoDrop 2000 (Thermo Scientific), and complementary DNA (cDNA) was produced using the High Capacity RNA-to-cDNA kit (Life Technologies). TaqMan Universal Master Mix II and TaqMan Gene Expression Assays (Life Technologies) were used to assess gene expression (Supplementary Table S1; Supplementary Data are available online at www.liebertpub.com/tec). The quantitative PCR (qPCR) reactions were performed using the CFX96 Real-Time PCR Detection System (Bio-Rad). All reactions were performed in duplicate using 18S as an endogenous control gene and analyzed using the comparative C_t method,[35] normalizing the expression level to ECFC-ECs using the formula $2^{-\Delta\Delta Ct}$, where $\Delta\Delta C_t$ is described as $[(C_{t\ \text{gene of interest}} - C_{t\ 18S})_{\text{sample of interest}} - (C_{t\ \text{gene of interest}} - C_{t\ 18S})_{ECFC-EC}]$. The natural log of the ratio of ephrinB2

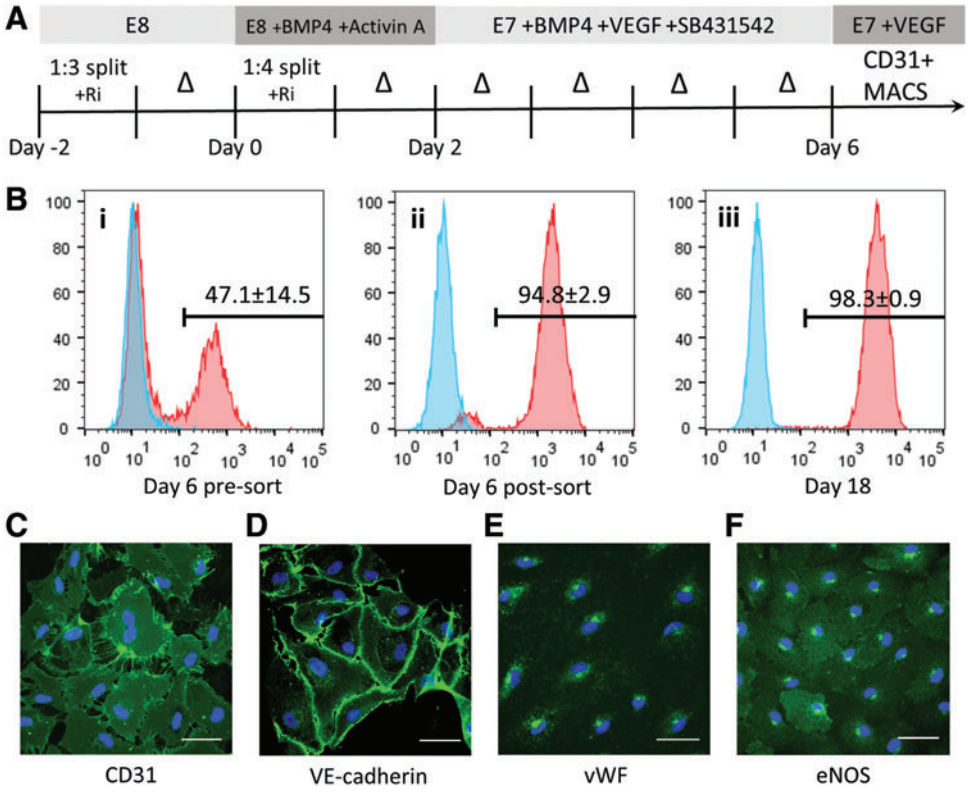

FIG. 1. Differentiation, isolation, and basic characterization of iPS-ECs. **(A)** Schematic of the iPS-EC differentiation protocol. The iPS-ECs were isolated using MACS for CD31 on day 6. **(B)** The differentiated cells were analyzed for CD31 expression by flow cytometry on day 6 **(i)** before sorting, **(ii)** after MACS sorting, and **(iii)** 12 days of culture after sorting. *Blue* = isotype control. The expression of definitive endothelial markers was confirmed using immunofluorescence for **(C)** CD31, **(D)** VE-cadherin, **(E)** vWF, and **(F)** eNOS. Scale bar: 50 μm. eNOS, endothelial nitric oxide synthase; iPS-EC, induced pluripotent stem cell-derived endothelial cells; VE, vascular endothelial; vWF, von Willebrand factor. Color images available online at www.liebertpub.com/tec

and EphB4 expression was used to represent arterial versus venous phenotype, as previously described.[36]

Microfluidic device fabrication and culture

The microfluidic device was fabricated using standard soft lithography and replica molding techniques, as described previously.[11,22,37] The devices were cast of polydimethylsiloxane (PDMS), plasma bonded onto glass slides, and sterilized before cell loading. For shear stress experiments, the devices were coated with fibronectin for 1 h at 37°C before introducing the cells at 2×10^7 cells/mL in a total volume of 2 μL. The cells were incubated for 2 h at 37°C before feeding with the E7V medium to flush out unattached cells. For the 3D vasculogenesis assays, the devices were loaded through the side-loading channel with 1×10^7 iPS-EC/mL and 5×10^6 NHLF/mL in 10 mg/mL fibrinogen (Sigma-Aldrich) and 0.25 U/mL aprotinin (Sigma-Aldrich) in 7.5 μL volume mixed with 0.9 μL of thrombin (3 U/mL final concentration; Sigma-Aldrich). The fibrin gel was polymerized for 15 min at 37°C before coating the fluidic lines with fibronectin (100 μg/mL). The devices were incubated for an additional 15 min at 37°C before feeding with endothelial growth medium 2 (EGM-2; Lonza) containing 0.25 U/mL aprotinin.

Vasculogenesis device analysis

The cocultured iPS-ECs and NHLF were imaged and fed with EGM-2 every 2 days, with alternating interstitial flow directions using a 5 mm H_2O hydrostatic pressure difference across the tissue chambers. Where indicated, SB431542 or sunitinib was supplemented at concentrations of 10 and 0.1 μM, respectively. The barrier function of the vasculature was tested by introducing 70 kDa FITC dextran (Molecular Probes) or fluorescent 1 μm diameter FluoSpheres® microspheres (Molecular Probes) through the media channel. The devices were fixed for immunofluorescence on day 14. For vessel area quantification, a region of interest (ROI) was selected to outline the chamber using ImageJ (National Institutes of Health [NIH]). A Gaussian blur was applied to reduce noise; then, the image was thresholded to create a binary image. The erode function was used to further reduce noise, and the area was measured within the ROI. For vessel length quantification, segmented lines were manually traced over the vessels within the ROI. The ratio of the vessel area and the vessel length was used to quantify the average vessel diameter. Each of the three chambers within the microfluidic device was analyzed separately, and each experimental condition consisted of at least three independent devices. The images were blinded for analysis.

Statistical analysis

All experiments were performed using at least three biological replicates. Significance was calculated using one-way analysis of variance (ANOVA) in conjunction with Tukey's multiple comparison test or Dunnett's multiple comparison test, with p-values <0.05 considered statistically significant. For the vessel analysis, two-way ANOVA in conjunction with Sidak's multiple comparison test was used. All results are reported as mean ± standard deviation. Data were compiled, analyzed, and graphed using Microsoft Excel and GraphPad Prism 6.

Additional information and explanation of methods can be found in the Supplementary Data.

Results

Physiological characterization of iPS-ECs

The iPS-ECs were differentiated using a monolayer, serum-free differentiation protocol as diagramed (Fig. 1A).

Day 6 of differentiation yielded a cell population that was $47.1\% \pm 14.5\%$ $CD31^+$ (Fig. 1Bi) before magnetic sorting. Following magnetic sorting, the cell population was purified to $94.8\% \pm 2.9\%$ $CD31^+$ (Fig. 1Bii). The cells were then grown on fibronectin-coated tissue culture plastic, and an additional 12 days of culture further enriched for iPS-ECs, yielding $98.3\% \pm 0.9\%$ $CD31^+$ cells (Fig. 1Biii). The sorted iPS-EC population also expressed the endothelial progenitor cell (EPC) marker CD34 ($82.4\% \pm 9.6\%$), while a small subpopulation stained positively for another EPC marker CD133 ($5.90\% \pm 1.11\%$) (Supplementary Fig. S1A, B). The cells did not express the hematopoietic marker CD45 ($0.87\% \pm 0.19\%$), while staining positively for the mesenchymal marker CD90 ($93.2\% \pm 3.39\%$), which has previously been shown to be expressed in EPCs (Supplementary Fig. S1C, D).[38,39] The resulting cells demonstrated a ''cobblestone'' morphology characteristic of primary endothelial cells, including HUAECs, HUVECs, HDLECs, and ECFC-ECs (Supplementary Fig. S2A). These cells also had protein expression characteristic of endothelial cells, including expression of CD31 and VE-cadherin that predominantly colocalized at cell junctions (Fig. 1C, D) and cytoplasmic expression of vWF and eNOS (Fig. 1E, F). ECFC-ECs were used as positive control, while isotype IgG antibodies were used as negative controls (Supplementary Fig. S2B, C). Successful differentiation and isolation was achieved using two different human iPSC lines (Supplementary Fig. S2D). The iPS-ECs thawed from day 8 of differentiation underwent an approximately sevenfold increase in cell number before undergoing senescence (Supplementary Fig. S2E). Culturing the iPS-ECs in EGM-2 instead of the E7V medium resulted in observable dedifferentiation of the iPS-ECs into cells of stromal- or smooth muscle-like morphology (Supplementary Fig. S2F).

Phenotypic characterization of iPS-ECs

In addition to the definitive endothelial markers, we investigated the expression of markers that define arterial, venous, and lymphatic endothelial phenotype. We specifically measured the ratio of the expression of the putative arterial and venous markers (ephrinB2 and EphB4, respectively).[40,41] The results were compared to primary human endothelial cells of known phenotype and normalized to ECFC-ECs as the progenitor endothelial cell control. As expected, the HUAECs had a more arterial-like phenotype compared to ECFC-ECs (higher ratio of ephrinB2 to EphB4), while HUVECs and HDLECs had a more venous-like phenotype (Fig. 2A). The iPS-ECs also demonstrated a strong venous phenotype compared to ECFC-ECs (Fig. 2A). To distinguish between venous and lymphatic endothelial phenotype, we investigated the expression of three different lymphatic endothelial markers: lymphatic vessel endothelial hyaluronan receptor-1 (LYVE-1), prospero homeobox protein 1 (PROX1), and podoplanin (PDPN). As expected, the HDLECs showed a positive expression of all three markers (Fig. 2B). The iPS-ECs showed low expression of PDPN and PROX1, but showed high expression of LYVE-1 (Fig. 2B). A similar expression pattern was observed for the ECFC-ECs (Fig. 2B). The expression pattern of the lymphatic markers for iPS-ECs and HDLECs was confirmed using immunofluorescence (Fig. 2C).

CDH5-*mCherry iPSC line*

Using CRISPR/Cas9, we established a mCherry-VE-cadherin reporter iPSC line. The iPS-ECs derived from the *CDH5*-mCherry iPSC line (*CDH5*-iPS-EC) demonstrated robust mCherry signal that colocalized to the cell junctions, as well as an accumulation of the signal near the cell nucleus (Fig. 3A). Since VE-cadherin is involved in maintaining endothelial barrier function,[42] we investigated whether the fusion protein impacted the permeability of the *CDH5*-iPS-EC monolayer. Using a Transwell permeability assay, we observed no statistically significant difference in the diffusion of 70 kDa dextran between the *CDH5*-iPS-ECs, iPS-ECs, and ECFC-ECs (Fig. 3B). All three EC types demonstrated significantly lower permeability of 70 kDa dextran compared to fibroblasts, with permeability values comparable to previous studies using primary VE cells ($4.73 \times 10^{-6} \pm 0.85 \times 10^{-6}$ cm/s for *CDH5*-iPS-ECs) (Fig. 3B).[43,44] We also studied the ability of *CDH5*-iPS-ECs to form tube-like structures on Matrigel (Fig. 3C). Again, we observed no statistically significant difference between *CDH5*-iPS-ECs, iPS-ECs, and ECFC-ECs (Fig. 3D). In addition, we tested the physiological response of *CDH5*-iPS-ECs to thrombin, which induces EC retraction through the redistribution of VE-cadherin.[45] Time-lapse imaging of the *CDH5*-iPS-ECs showed dissociation of the mCherry-VE-cadherin signal at cell junctions in response to thrombin, resulting in EC retraction and formation of intercellular gaps (Fig. 3E and Supplementary Video S1).

iPS-EC response to shear stress

Using the *CDH5*-iPS-ECs, we investigated the cellular response to an applied shear stress. We utilized a microfluidic device that consisted of microfluidic lines 10 mm in length with cross-sectional dimensions of 800 and 100 μm in width and height, respectively. Using finite element modeling to determine the fluid shear stress, we set the fluid flow within the line to produce an average shear stress of 4 dynes/cm^2 (Supplementary Fig. S3). The cells were observed using time-lapse imaging of the mCherry-VE-cadherin signal, and morphological changes were observed over the course of 20 h (Fig. 3E). Using circularity as a morphological index, we observed significant elongation of the cells in response to shear stress (Fig. 3F).

Three-dimensional iPS-EC vascular networks

We next investigated the ability of *CDH5*-iPS-ECs to form 3D vascular networks by coculturing them with fibroblasts in microfluidic devices (Fig. 4A). Using the mCherry-VE-cadherin signal to track vessel formation, we observed the development of a robust vessel network over the course of 14 days (Fig. 4B and quantitative analysis in Fig. 5). The iPS-ECs undergo vacuole formation and aggregate into tube-like structures in the first 48 h, as previously observed using primary ECs (Supplementary Fig. S4A).[46] The microvessel network connected to the top and bottom microfluidic lines (Fig. 4C), enabling the flow of media through the vascular networks without leakage into the surrounding tissue space. The vessels have a complete lumen as confirmed by staining for CD31 and imaging using confocal microscopy (Fig. 4D). Costaining for laminin, a basement membrane protein, we observed the localization of laminin on the outer wall of the

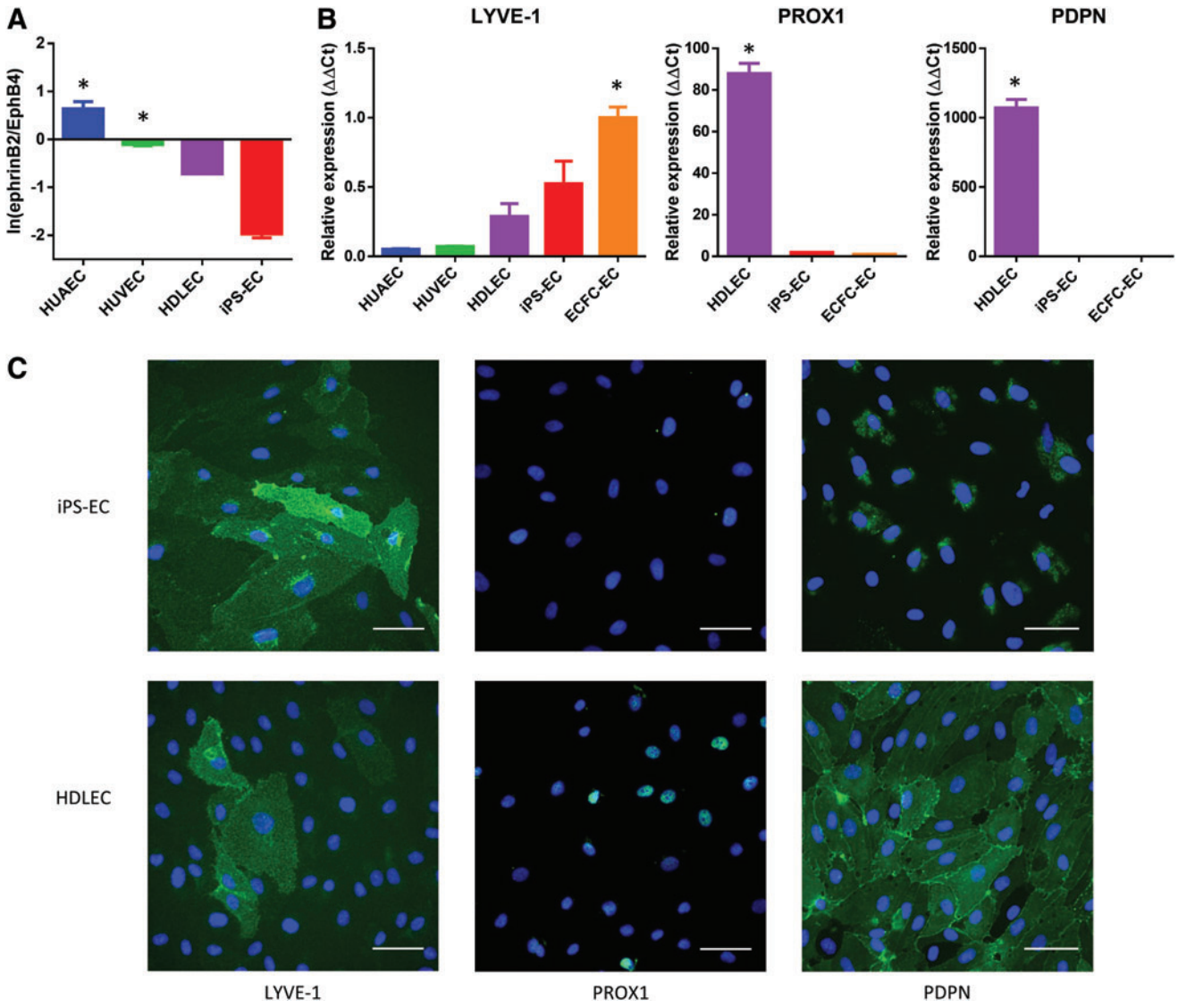

FIG. 2. Phenotype characterization of iPS-ECs. **(A)** The ratio of ephrinB2 to EphB4 expression levels measured by qPCR. The expression levels are normalized to ECFC-ECs, with values >0 indicating a more arterial phenotype than ECFC-ECs. HUVECs, HDLECs, and iPS-ECs demonstrate a more venous phenotype than ECFC-ECs. *$p < 0.05$ compared to iPS-ECs. **(B)** Expression levels of lymphatic markers measured by qPCR, normalized to ECFC-ECs. *$p < 0.05$ compared to iPS-ECs. **(C)** Expression of lymphatic markers confirmed by immunofluorescence. The HDLECs stain positively for all three markers, while the iPS-ECs only stain positively for LYVE-1. *Blue* = DAPI. Scale bar: 50 μm. DAPI, 4′,6-diamidino-2-phenylindole, dihydrochloride; ECFC-EC, endothelial colony-forming cell-derived endothelial cell; HDLECs, human dermal lymphatic endothelial cells; HUVECs, human umbilical vein endothelial cells; LYVE-1, lymphatic vessel endothelial hyaluronan receptor-1; qPCR, quantitative polymerase chain reaction. Color images available online at www.liebertpub.com/tec

microvessels as outlined by CD31 (Fig. 4E). The vascular network demonstrates a physiological barrier function, as they effectively retain fluorescently labeled 70 kDa dextran (Fig. 4F). Furthermore, we were able to flow 1 μm beads through the vessels (Fig. 4G).

Supplementation of small molecule TGF-β inhibitor

Since TGF-β inhibition has an established effect of enhancing iPS-EC proliferation in monolayer culture,[47] we explored whether TGF-β inhibition also leads to improved vessel network formation. A small molecule TGF-β inhibitor (SB431542) was supplemented into the growth medium and the vessel formation was compared to the control condition (Fig. 5A). The addition of SB431542 resulted in a significant increase in vessel length (26–49%) at all measured time points (days 6, 10, and 14) (Fig. 5B). The increase in vessel area (23–57%) was statistically significant for days 6 and 10 and showed a strong positive trend for day 14 ($p = 0.12$) (Fig. 5C). No statistically significant difference in the average vessel diameter was observed at all three time points (Fig. 5D).

Vessel response to antiangiogenic drug

To further demonstrate the utility of the platform, we investigated the effects of the antiangiogenic drug sunitinib.

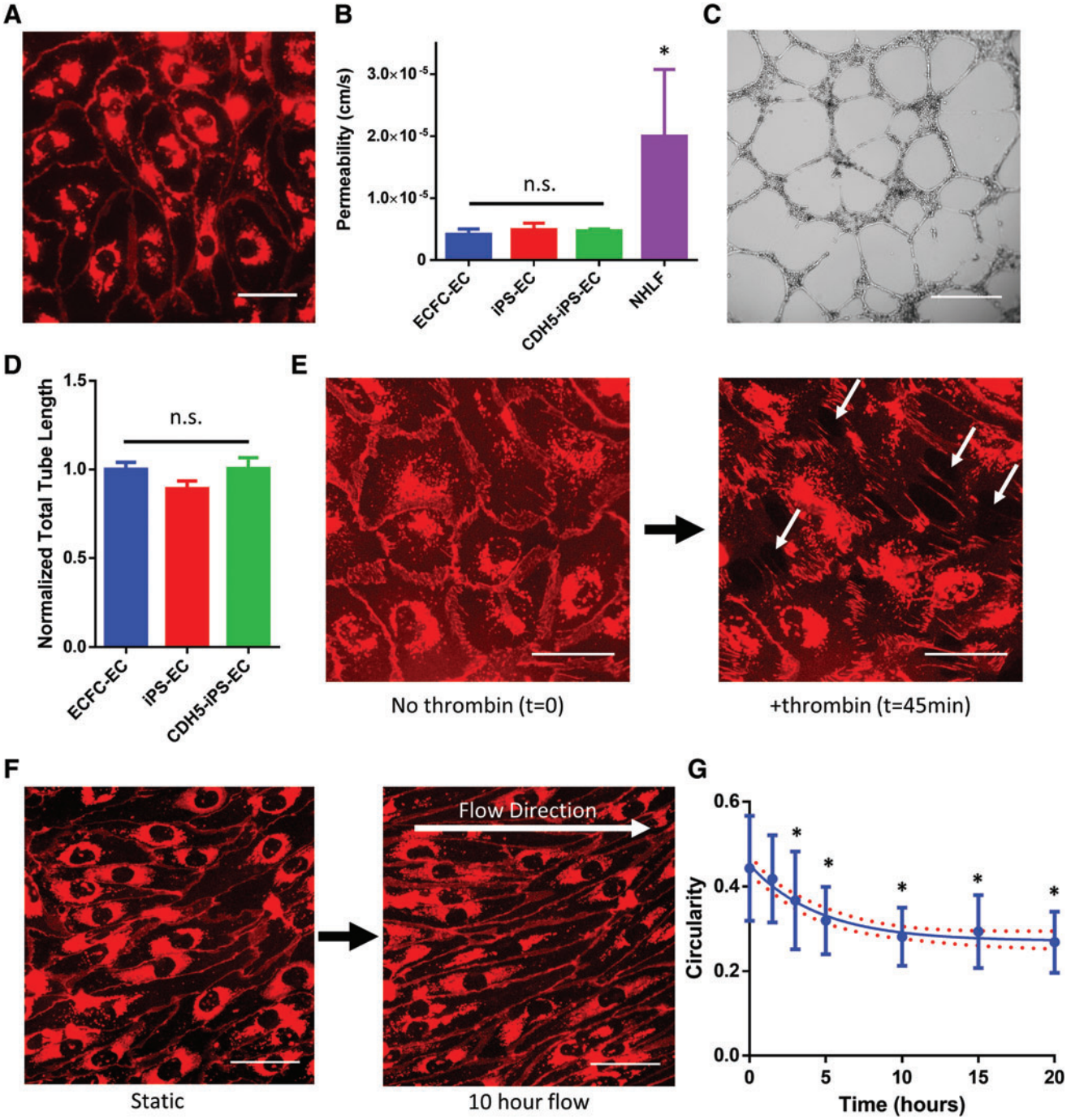

FIG. 3. The use of *CDH5*-mCherry iPSC-derived ECs (*CDH5*-iPS-ECs). **(A)** The *CDH5*-iPS-ECs demonstrate mCherry signal that localizes to cell junctions. **(B)** The permeability measured by the diffusion of 70 kDa dextran across a cell monolayer. The permeability of *CDH5*-iPS-EC monolayer is unchanged compared to iPS-ECs as well as ECFC-ECs. $^*p < 0.05$ compared to *CDH5*-iPS-ECs. **(C)** Representative image of Matrigel tube formation assay for *CDH5*-iPS-ECs. **(D)** The total tube length normalized to ECFC-ECs. No significant differences were observed across the three EC types. **(E)** *CDH5*-iPS-EC response to thrombin. The mCherry-VE-cadherin disaggregate from cell junctions, resulting in the formation of intercellular gaps (indicated by *white arrows*). **(F)** The *CDH5*-iPS-ECs are used to image the response to shear stress in real time. The cells demonstrate a more elongated morphology over time. **(G)** The circularity of the *CDH5*-iPS-ECs in response to shear stress is calculated over time. $^*p < 0.05$ compared to time 0. *Line* indicates a one-phase decay fit with 95% confidence band. Scale bar: 50 μm **(A, E, F)**, 500 μm **(C)**. Color images available online at www.liebertpub.com/tec

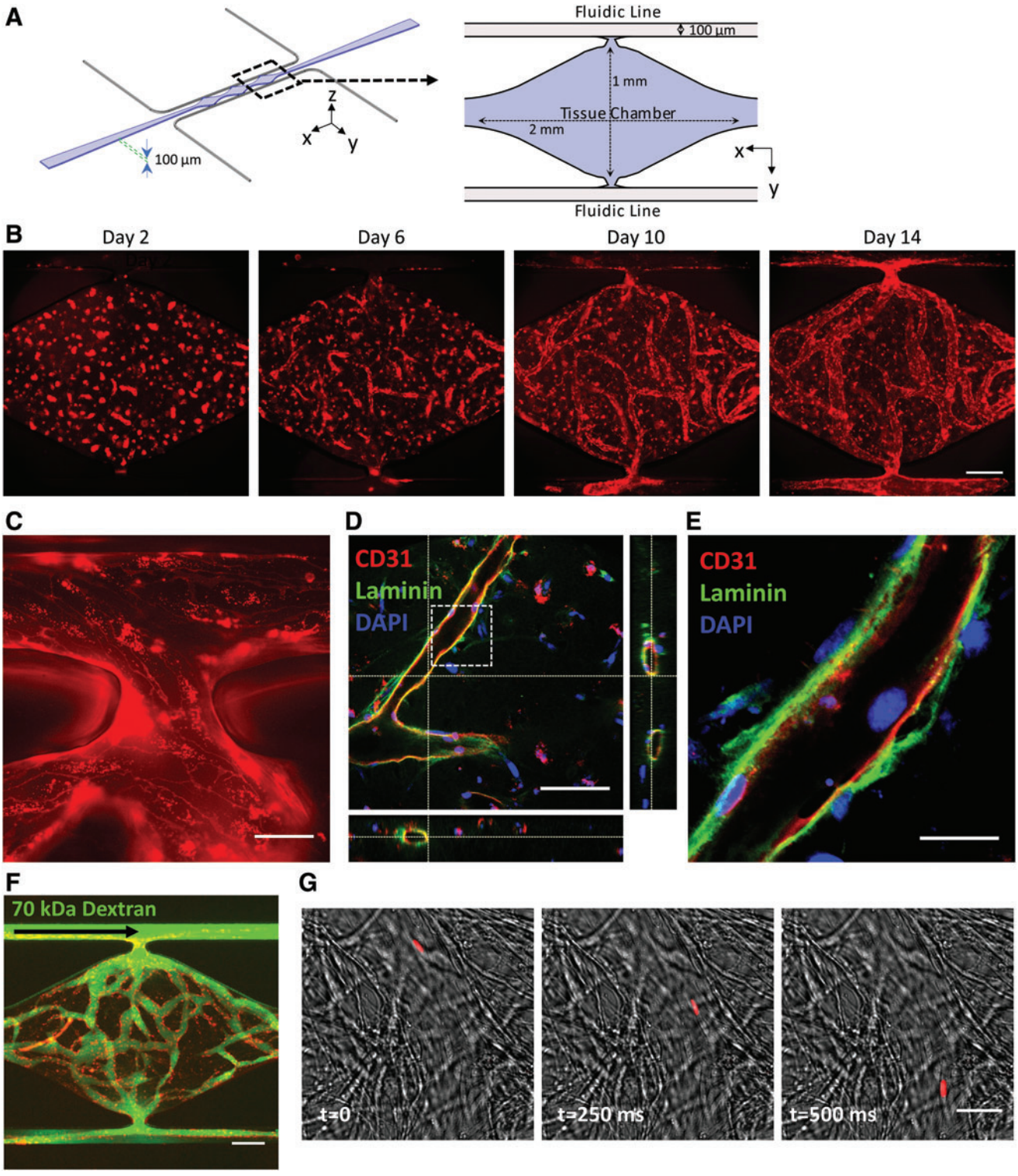

FIG. 4. Three-dimensional culture of iPS-ECs in microfluidic devices. **(A)** Schematic illustration of the microfluidic device. The cell suspension in fibrin is loaded into the tissue chamber region, while media are delivered through the *top* and *bottom* fluidic *lines*. **(B)** Representative images of the vessel network formation by *CDH5*-iPS-ECs tracked over a period of 14 days. **(C)** The vessel anastomoses to the *top* fluidic *line* as indicated by the continuous *CDH5*-iPS-EC lining around the opening of the tissue chamber. **(D)** The microvessels demonstrate a patent lumen as confirmed by confocal microscopy. The *dashed box* region: **(E)** the iPS-ECs deposit laminin as a part of the basement membrane. **(F)** The vessel network effectively retains 70 kDa dextran introduced through the *top* fluidic *line*. **(G)** One micrometer bead (*red*) is captured flowing through the vessel. Scale bar: 200 µm **(B, F)**, 50 µm **(C)**, 100 µm **(D)**, 25 µm **(E, G)**. Color images available online at www.liebertpub.com/tec

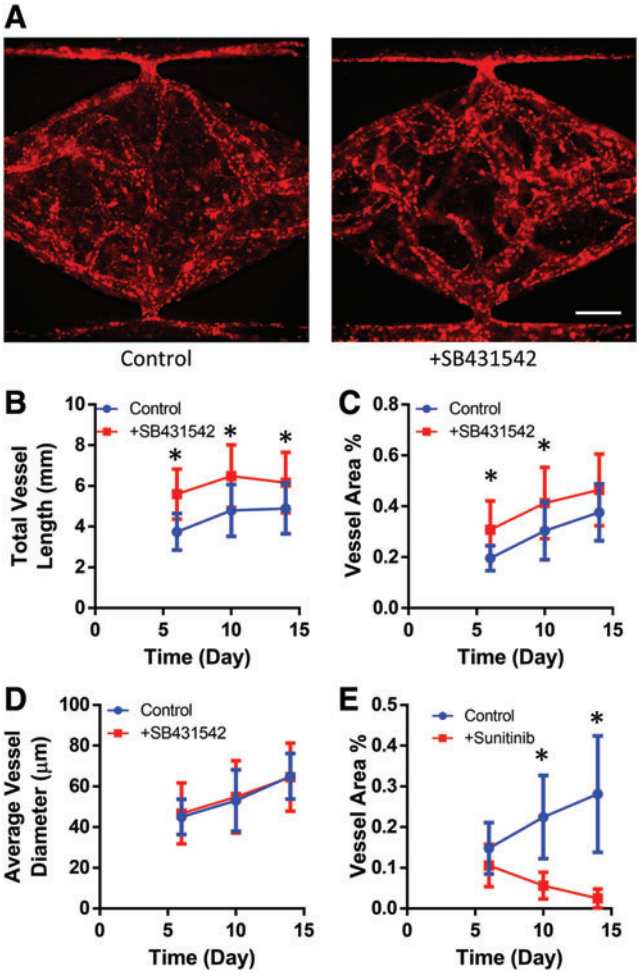

FIG. 5. Response of iPS-EC vasculature to small molecule inhibitors. **(A)** Representative *CDH5*-iPS-EC vessel networks developed at day 14 with or without the supplementation of SB431542 in the growth medium. The addition of SB432542 significantly increased **(B)** the total vessel length and **(C)** the total vessel area coverage within the tissue chamber. $*p<0.05$ compared to control at the given time point. **(D)** The average vessel diameter is not significantly affected by the addition of SB431542. **(E)** The total vessel area within the tissue chamber decreases in response to sunitinib treatment. $*p<0.05$ comparing control versus sunitinib-treated condition at the given time point. Color images available online at wwwliebertpub.com/tec

Sunitinib is a multitargeted tyrosine kinase inhibitor used for cancer treatment due to its antiangiogenic and antitumor activities.[48,49] On day 6 of culture, sunitinib was added to the medium at 100 nM, and we observed a statistically significant reduction in the total vessel area compared to control (Fig. 5E).

Discussion

In this study, we characterized critical physiological functions of iPS-ECs using two-dimensional (2D) and 3D *in vitro* cultures. The iPS-ECs demonstrated the expression of several definitive endothelial cell markers and maintained this expression pattern even after 12 days of culture in a serum-free medium. We established a novel *CDH5*-iPS-EC line expressing the mCherry-VE-cadherin fusion protein, which was used to perform live cell imaging at various time points over the course of a single experiment. The gene expression pattern of the iPS-ECs suggests a venous-like endothelial phenotype compared to ECFC-ECs. The iPS-EC monolayer demonstrates physiological barrier functions, a shear stress response, and the ability to form vessel structures when cultured on Matrigel. In 3D, the iPS-ECs are capable of undergoing vasculogenic and angiogenic processes to form robust, perfusable vascular networks. Finally, we demonstrate that the iPS-EC vascular networks are responsive to small molecule inhibitors that have angiogenic or antiangiogenic effects. Thus, the *CDH5*-iPS-EC line provides a convenient yet robust model that is consistent with the physiological characteristics of primary ECs. Based on their ability to form 3D perfused vascular networks, we believe iPS-ECs have the potential to be used in a wide range of *in vitro* and *in vivo* tissue engineering applications.

The iPS-EC differentiation protocol utilized in this study has several advantages compared to several previously established differentiation protocols. The differentiation does not vary in technique from the standard monolayer, feeder-free culture of hPSCs, requiring no additional steps for embryoid body formation or suspension culture. The differentiation and maintenance media are serum free, which minimize the variability in the differentiation protocol. Bao *et al.*[50] recently reported the successful differentiation of human iPS-ECs using chemically defined, albumin-free media and xenogen-free substrate (Synthemax vitronectin). While their reported differentiation efficiency is lower than achieved in this study (~30% vs. ~45%), further advancements in chemically defined differentiation protocols could further improve reproducibility and translational applications.

In addition, selecting an appropriate iPS-EC differentiation strategy requires careful consideration of the intended application and function of the tissue. While the iPS-ECs derived in this study demonstrated a predominantly venous phenotype, previous studies have reported a more arterial phenotype, especially when cultured in high concentrations of VEGF-A.[51–53] Other groups have reported an indeterminate phenotype, which may be an indication of the immaturity of iPS-ECs.[36,54] Differences are likely due to the distinct differentiation protocols utilized by the different research groups, highlighting the sensitivity in differentiating ECs from hPSCs and that further work is needed to better control this process. The expression of LYVE-1 without the expression of other lymphatic markers is consistent with previous findings.[47,54] It has been shown that LYVE-1 expression is not limited to lymphatic ECs,[55] and the lack of expression of PROX1 and PDPN strongly suggests that the iPS-ECs in our study are indeed more venous like and not lymphatic. It remains to be seen how the phenotype-specific functions of iPS-ECs will influence their potential applications in MPS. In addition to the basic phenotype of the iPS-ECs, it will be critical to consider organ- and tissue-specific functions of endothelial cells to further advance the capabilities of MPS to model the *in vivo* microenvironment.[2,29,56]

We established a *CDH5*-mCherry human iPSC line that can be utilized to generate iPS-ECs expressing an mCherry-VE-cadherin fusion protein. While we did not detect any dysregulation in the *CDH5*-iPS-EC barrier function or

response to thrombin, we observed mCherry signal accumulation around the cell nucleus. We believe that this cytoplasmic mCherry signal is due to VE-cadherin internalization, as VE-cadherin has known mechanisms of endocytosis in response to signaling factors such as VEGF and thrombin.[45,57] Indeed, some of the mCherry signal can be observed entering the cytoplasm of the cell in response to thrombin (Supplementary Video S1). Similar observations of signal accumulation were made in previous works using HUVECs that expressed fluorescently labeled VE-cadherin by lentiviral transduction.[58,59] While efficient, lentiviral systems have significant shortcomings, as the gene encoding the fusion protein is randomly inserted into the genome and the expression of the protein is forced through a promoter sequence. The *CDH5*-mCherry iPSC line utilized CRISPR/Cas9 to specifically modify the *CDH5* gene; thus, the mCherry signal is only observed in cells that express VE-cadherin using the native promoter. Further genetic modifications can be made on the *CDH5*-iPSC line to perform mechanistic studies on VE-cadherin and its role in EC physiology and pathophysiology.

While the iPS-ECs formed 3D vessel networks within the microfluidic device, we utilized a relatively high density of iPS-ECs (1×10^7 cells/mL) to achieve consistent vascular network formation. We observed that the iPS-ECs loaded at the same concentration as previous experiments using ECFC-ECs (5×10^6 cells/mL) resulted in fragmented vessel networks that did not consistently form a continuous vessel network across the top and bottom fluidic lines (Supplementary Fig. S4B). In addition, we observed a large number of iPS-ECs within the device that did not integrate into vessel networks. These data suggest that the iPS-ECs have a limited vasculogenic potential compared to the ECFC-ECs and the iPS-EC population may include poorly differentiated cells that have vasculogenic deficiencies. While the iPS-ECs express CD31, additional markers may be necessary to select for a highly vasculogenic iPS-EC subpopulation. For example, neuropilin-1 (NRP-1) is a marker that has been shown to select for a human iPS-EC subpopulation that shows high proliferative capacity and robust vessel network formation *in vivo*.[24,60] Hu *et al.*[61] recently reported that iPS-ECs differentiated from an iPSC line that originates from ECs (as opposed to fibroblasts) have higher expression of EC markers, suggesting that the cellular origin of the iPSCs may also play a role in iPS-EC functionality. Additional studies are necessary to investigate how to enrich for highly vasculogenic iPS-ECs. The data also highlight the inability of the Matrigel tube formation assay to assess vasculogenic potential of ECs, as no significant difference between the ECFC-ECs and iPS-ECs was detected.

Our investigations of the microvessels formed by the iPS-ECs demonstrate features of a mature vasculature. The microvessels demonstrate a continuous basement membrane that stained positively for laminin, a key extracellular matrix (ECM) protein involved in vessel stabilization and maturation.[62] This is in contrast to the iPS-ECs cultured in a 2D monolayer where laminin staining is discontinuous and localizes around the nucleus (Supplementary Fig. S5), as similarly observed in a previous study.[63] It is also interesting to note that the iPS-ECs in the device were cultured using EGM-2 for 14 days, a condition under which the iPS-ECs cultured in a 2D monolayer showed a propensity to dedifferentiate into cells with a stromal phenotype. These data suggest that the 3D culture of the iPS-ECs in the presence of fibroblasts can enhance the phenotypic commitment of the iPS-ECs. Cytokines released by fibroblasts have been demonstrated as a critical component in the formation of stable microvessels *in vitro*.[13,64] Further studies are required to establish if these cytokines enhance the differentiation and maturation of iPS-ECs.

We demonstrated that the iPS-EC vessel network formation can be improved by the addition of a small molecule TGF-β inhibitor SB431542in the culture medium. SB431542 inhibits TGF-β signaling by blocking activin-like kinase (ALK) receptors[65] and is commonly used to enhance EC differentiation and expansion.[34,36,47,54,66] Using 2D tube formation assays, previous studies have shown that the addition of SB431542 in the culture medium can enhance area of coverage and total branch number of iPS-ECs.[54,66] A similar response is observed in our 3D vasculogenesis assay using iPS-ECs, as the addition of SB431542 results in significant increases in both the total vessel area and the total vessel length. No significant increase in the average vessel diameter was observed, indicating that the increased branching of the vasculature leads to an increased total vessel area.

In conclusion, this study advances the current understanding of iPS-ECs and their utility in creating advanced MPS. The iPS-ECs demonstrate physiological functions in both 2D and 3D culture, and can be manipulated to create robust microvascular networks in microfluidic devices. By understanding the basic characteristics and behavior of iPS-ECs, the tissue engineering community can make informed decisions on the integration of iPS-ECs in advancing MPS as well as other tissue engineering platforms.

Acknowledgments

The authors acknowledge the GEiC, Washington University in St. Louis, for creating the *CDH5*-mCherry iPSC line. The authors thank Christina Tu and Dr. Leslie Lock, University of California, Irvine, for their assistance in the iPS-EC differentiation protocol. This work was supported by the NIH (UH3-TR-000481) and the American Heart Association (16PRE30480019 to Y.K.K.).

Disclosure Statement

S.C.G. is a cofounder of 4Design Biosciences, LLC. All other authors have no competing financial interests.

References

1. Cleaver, O., and Melton, D.A. Endothelial signaling during development. Nat Med **9,** 661, 2003.
2. Rafii, S., Butler, J.M., and Ding, B.-S. Angiocrine functions of organ-specific endothelial cells. Nature **529,** 316, 2016.
3. Deanfield, J.E., Halcox, J.P., and Rabelink, T.J. Endothelial function and dysfunction: testing and clinical relevance. Circulation **115,** 1285, 2007.
4. Heylman, C., Sobrino, A., Shirure, V.S., Hughes, C.C., and George, S.C. A strategy for integrating essential three-dimensional microphysiological systems of human organs for realistic anticancer drug screening. Exp Biol Med **239,** 1240, 2014.

5. Esch, M.B., Smith, A.S.T., Prot, J.-M., Oleaga, C., Hickman, J.J., and Shuler, M.L. How multi-organ microdevices can help foster drug development. Adv Drug Deliv Rev **69–70,** 158, 2014.
6. Bhatia, S.N., and Ingber, D.E. Microfluidic organs-on-chips. Nat Biotechnol **32,** 760, 2014.
7. Passier, R., Orlova, V., and Mummery, C. Complex tissue and disease modeling using hiPSCs. Cell Stem Cell **18,** 309, 2016.
8. Bogorad, M.I., DeStefano, J., Karlsson, J., Wong, A.D., Gerecht, S., and Searson, P.C. Review: in vitro microvessel models. Lab Chip **15,** 4242, 2015.
9. Morin, K.T., and Tranquillo, R.T. In vitro models of angiogenesis and vasculogenesis in fibrin gel. Exp Cell Res **319,** 2409, 2013.
10. Sun, X., Altalhi, W., and Nunes, S.S. Vascularization strategies of engineered tissues and their application in cardiac regeneration. Adv Drug Deliv Rev **96,** 183, 2016.
11. Moya, M.L., Hsu, Y.-H., Lee, A.P., Hughes, C.C.W., and George, S.C. In vitro perfused human capillary networks. Tissue Eng Part C Methods **19,** 730, 2013.
12. Kim, S., Lee, H., Chung, M., and Jeon, N.L. Engineering of functional, perfusable 3D microvascular networks on a chip. Lab Chip **13,** 1489, 2013.
13. Whisler, J.a., Chen, M.B., and Kamm, R.D. Control of perfusable microvascular network morphology using a multiculture microfluidic system. Tissue Eng Part C Methods **20,** 543, 2014.
14. Wang, X., Phan, D.T.T., Sobrino, A., George, S.C., Hughes, C.C.W., and Lee, A.P. Engineering anastomosis between living capillary networks and endothelial cell-lined microfluidic channels. Lab Chip **16,** 282, 2016.
15. Alonzo, L.F., Moya, M.L., Shirure, V.S., and George, S.C. Microfluidic device to control interstitial flow-mediated homotypic and heterotypic cellular communication. Lab Chip **15,** 3521, 2015.
16. Kim, S., Chung, M., Ahn, J., Lee, S., and Jeon, N.L. Interstitial flow regulates the angiogenic response and phenotype of endothelial cells in a 3D culture model. Lab Chip **16,** 4189, 2016.
17. Zanotelli, M.R., Ardalani, H., Zhang, J., Hou, Z., Nguyen, E.H., Swanson, S., *et al.* Stable engineered vascular networks from human induced pluripotent stem cell-derived endothelial cells cultured in synthetic hydrogels. Acta Biomater **35,** 32, 2016.
18. Belair, D.G., Whisler, J.A., Valdez, J., Velazquez, J., Molenda, J.A., Vickerman, V., *et al.* Human vascular tissue models formed from human induced pluripotent stem cell derived endothelial cells. Stem Cell Rev **11,** 511, 2015.
19. Bersini, S., Jeon, J.S., Dubini, G., Arrigoni, C., Chung, S., Charest, J.L., *et al.* A microfluidic 3D in vitro model for specificity of breast cancer metastasis to bone. Biomaterials **35,** 2454, 2014.
20. Jeon, J.S., Bersini, S., Gilardi, M., Dubini, G., Charest, J.L., Moretti, M., *et al.* Human 3D vascularized organotypic microfluidic assays to study breast cancer cell extravasation. Proc Natl Acad Sci U S A **112,** 214, 2015.
21. Moya, M., Tran, D., and George, S.C. An integrated in vitro model of perfused tumor and cardiac tissue. Stem Cell Res Ther **4**(Suppl 1), S15, 2013.
22. Sobrino, A., Phan, D.T.T., Datta, R., Wang, X., Hachey, S.J., Romero-López, M., *et al.* 3D microtumors in vitro supported by perfused vascular networks. Sci Rep **6,** 31589, 2016.
23. Miyaoka, Y., Chan, A.H., Judge, L.M., Yoo, J., Huang, M., Nguyen, T.D., *et al.* Isolation of single-base genome-edited human iPS cells without antibiotic selection. Nat Methods **11,** 291, 2014.
24. Samuel, R., Daheron, L., Liao, S., Vardam, T., Kamoun, W.S., Batista, A., *et al.* Generation of functionally competent and durable engineered blood vessels from human induced pluripotent stem cells. Proc Natl Acad Sci U S. A **110,** 12774, 2013.
25. Mordwinkin, N.M., Lee, A.S., and Wu, J.C. Patient-specific stem cells and cardiovascular drug discovery. JAMA **310,** 2039, 2013.
26. Qin, Y., and Gao, W.-Q. Concise review: patient-derived stem cell research for monogenic disorders. Stem Cells **34,** 44, 2016.
27. Clayton, Z.E., Sadeghipour, S., and Patel, S. Generating induced pluripotent stem cell derived endothelial cells and induced endothelial cells for cardiovascular disease modelling and therapeutic angiogenesis. Int J Cardiol **197,** 116, 2015.
28. Wong, W.T., Huang, N.F., Botham, C.M., Sayed, N., and Cooke, J.P. Endothelial cells derived from nuclear reprogramming. Circ Res **111,** 1363, 2012.
29. Wilson, H.K., Canfield, S.G., Shusta, E.V., and Palecek, S.P. Concise review: tissue-specific microvascular endothelial cells derived from human pluripotent stem cells. Stem Cells **32,** 3037, 2014.
30. Yoder, M.C. Differentiation of pluripotent stem cells into endothelial cells. Curr Opin Hematol **22,** 252, 2015.
31. Yoder, M.C., Mead, L.E., Prater, D., Krier, T.R., Mroueh, K.N., Li, F., *et al.* Redefining endothelial progenitor cells via clonal analysis and hematopoietic stem/progenitor cell principals. Blood **109,** 1801, 2007.
32. Lee, E.K., Kurokawa, Y.K., Tu, R., George, S.C., and Khine, M. Machine learning plus optical flow: a simple and sensitive method to detect cardioactive drugs. Sci Rep **5,** 11817, 2015.
33. Huebsch, N., Loskill, P., Mandegar, M.a., Marks, N.C., Sheehan, A.S., Ma, Z., *et al.* Automated video-based analysis of contractility and calcium flux in human-induced pluripotent stem cell-derived cardiomyocytes cultured over different spatial scales. Tissue Eng Part C Methods **21,** 467, 2015.
34. Schwartz, M.P., Hou, Z., Propson, N.E., Zhang, J., Engstrom, C.J., Costa, V.S., *et al.* Human pluripotent stem cell-derived neural constructs for predicting neural toxicity. Proc Natl Acad Sci U S A **112,** 12516, 2015.
35. Schmittgen, T.D., and Livak, K.J. Analyzing real-time PCR data by the comparative CT method. Nat Protoc **3,** 1101, 2008.
36. Kusuma, S., Peijnenburg, E., Patel, P., and Gerecht, S. Low oxygen tension enhances endothelial fate of human pluripotent stem cells. Arterioscler Thromb Vasc Biol **34,** 913, 2014.
37. Moya, M.L., Alonzo, L.F., and George, S.C. Microfluidic device to culture 3D in vitro human capillary networks. Methods Mol Biol **1202,** 21, 2013.
38. Zimmerlin, L., Donnenberg, V.S., Pfeifer, M.E., Meyer, E.M., Péault, B., Rubin, J.P., *et al.* Stromal vascular progenitors in adult human adipose tissue. Cytometry A **77A,** 22, 2009.
39. Park, T.S., Bhutto, I., Zimmerlin, L., Huo, J.S., Nagaria, P., Miller, D., *et al.* Vascular progenitors from cord blood-derived induced pluripotent stem cells possess augmented

capacity for regenerating ischemic retinal vasculature. Circulation **129,** 359, 2014.
40. Marcelo, K.L., Goldie, L.C., and Hirschi, K.K. Regulation of endothelial cell differentiation and specification. Circ Res **112,** 1272, 2013.
41. Atkins, G.B., Jain, M.K., and Hamik, A. Endothelial differentiation: molecular mechanisms of specification and heterogeneity. Arterioscler Thromb Vasc Biol **31,** 1476, 2011.
42. Dejana, E., Orsenigo, F., and Lampugnani, M.G. The role of adherens junctions and VE-cadherin in the control of vascular permeability. J Cell Sci **121,** 2115, 2008.
43. Lal, B.K., Varma, S., Pappas, P.J., Hobson, R.W., and Durán, W.N. VEGF increases permeability of the endothelial cell monolayer by activation of PKB/akt, endothelial nitric-oxide synthase, and MAP kinase pathways. Microvasc Res **62,** 252, 2001.
44. Siflinger-Birnboim, A., del Vecchio, P.J., Cooper, J.A., Blumenstock, F.A., Shepard, J.M., and Malik, A.B. Molecular sieving characteristics of the cultured endothelial monolayer. J Cell Physiol **132,** 111, 1987.
45. Rabiet, M.-J., Plantier, J.-L., Rival, Y., Genoux, Y., Lampugnani, M.-G., and Dejana, E. Thrombin-induced increase in endothelial permeability is associated with changes in cell-to-cell junction organization. Arterioscler Thromb Vasc Biol **16,** 488, 1996.
46. Davis, G.E., Bayless, K.J., and Mavila, A. Molecular basis of endothelial cell morphogenesis in three-dimensional extracellular matrices. Anat Rec **268,** 252, 2002.
47. James, D., Nam, H., Seandel, M., Nolan, D., Janovitz, T., Tomishima, M., *et al.* Expansion and maintenance of human embryonic stem cell-derived endothelial cells by TGFβ inhibition is Id1 dependent. Nat Biotechnol **28,** 161, 2010.
48. Demetri, G.D., van Oosterom, A.T., Garrett, C.R., Blackstein, M.E., Shah, M.H., Verweij, J., *et al.* Efficacy and safety of sunitinib in patients with advanced gastrointestinal stromal tumour after failure of imatinib: a randomised controlled trial. Lancet **368,** 1329, 2006.
49. Faivre, S., Demetri, G., Sargent, W., and Raymond, E. Molecular basis for sunitinib efficacy and future clinical development. Nat Rev Drug Discov **6,** 734, 2007.
50. Bao, X., Lian, X., Dunn, K.K., Shi, M., Han, T., Qian, T., *et al.* Chemically-defined albumin-free differentiation of human pluripotent stem cells to endothelial progenitor cells. Stem Cell Res **15,** 122, 2015.
51. White, M.P., Rufaihah, A.J., Liu, L., Ghebremariam, Y.T., Ivey, K.N., Cooke, J.P., *et al.* Limited gene expression variation in human embryonic stem cell and induced pluripotent stem cell-derived endothelial cells. Stem Cells **31,** 92, 2013.
52. Rufaihah, A.J., Huang, N.F., Kim, J., Herold, J., Volz, K.S., Park, T.S, *et al.* Human induced pluripotent stem cell-derived endothelial cells exhibit functional heterogeneity. Am J Transl Res **5,** 21, 2013.
53. Sriram, G., Tan, J.Y., Islam, I., Rufaihah, A.J., and Cao, T. Efficient differentiation of human embryonic stem cells to arterial and venous endothelial cells under feeder- and serum-free conditions. Stem Cell Res Ther **6,** 261, 2015.
54. Orlova, V.V., Drabsch, Y., Freund, C., Petrus-Reurer, S., van den Hil, F.E., Muenthaisong, S, *et al.* Functionality of endothelial cells and pericytes from human pluripotent stem cells demonstrated in cultured vascular plexus and zebrafish xenografts. Arterioscler Thromb Vasc Biol **34,** 177, 2014.
55. Baluk, P., and McDonald, D.M. Markers for microscopic imaging of lymphangiogenesis and angiogenesis. Ann N Y Acad Sci **1131,** 1, 2008.
56. Aird, W.C. Phenotypic heterogeneity of the endothelium: I. structure, function, and mechanisms. Circ Res **100,** 158, 2007.
57. Gavard, J., and Gutkind, J.S. VEGF controls endothelial-cell permeability by promoting the β-arrestin-dependent endocytosis of VE-cadherin. Nat Cell Biol **8,** 1223, 2006.
58. Breslin, J.W., Zhang, X.E., Worthylake, R.A., and Souza-Smith, F.M. Involvement of local lamellipodia in endothelial barrier function. PLoS One **10,** e0117970, 2015.
59. Taha, A.A., Taha, M., Seebach, J., and Schnittler, H.-J. ARP2/3-mediated junction-associated lamellipodia control VE-cadherin-based cell junction dynamics and maintain monolayer integrity. Mol Biol Cell **25,** 245, 2014.
60. Prasain, N., Lee, M.R., Vemula, S., Meador, J.L., Yoshimoto, M., Ferkowicz, M.J., *et al.* Differentiation of human pluripotent stem cells to cells similar to cord-blood endothelial colony-forming cells. Nat Biotechnol **32,** 1151, 2014.
61. Hu, S., Zhao, M.-T., Jahanbani, F., Shao, N.-Y., Lee, W.H., Chen, H., *et al.* Effects of cellular origin on differentiation of human induced pluripotent stem cell-derived endothelial cells. JCI Insight **1,** 1, 2016.
62. Davis, G.E. Endothelial extracellular matrix: biosynthesis, remodeling, and functions during vascular morphogenesis and neovessel stabilization. Circ Res **97,** 1093, 2005.
63. Kusuma, S., Facklam, A., and Gerecht, S. Characterizing human pluripotent-stem-cell-derived vascular cells for tissue engineering applications. Stem Cells Dev **24,** 451, 2015.
64. Nakatsu, M.N., Sainson, R.C.A., Aoto, J.N., Taylor, K.L., Aitkenhead, M., Pérez-del-Pulgar, S., *et al.* Angiogenic sprouting and capillary lumen formation modeled by human umbilical vein endothelial cells (HUVEC) in fibrin gels: the role of fibroblasts and angiopoietin-1. Microvasc Res **66,** 102, 2003.
65. Inman, G.J. SB-431542 Is a potent and specific inhibitor of transforming growth factor-beta superfamily type I activin receptor-like kinase (ALK) receptors ALK4, ALK5, and ALK7. Mol Pharmacol **62,** 65, 2002.
66. Bai, H., Gao, Y., Hoyle, D.L., Cheng, T., and Wang, Z.Z. Suppression of Transforming growth factor-β signaling delays cellular senescence and preserves the function of endothelial cells derived from human pluripotent stem cells. Stem Cells Transl Med **6,** 589, 2017.

Address correspondence to:
Steven C. George, MD, PhD
Department of Biomedical Engineering
Washington University in St. Louis
One Brookings Drive
St. Louis, MO 63130-1097

E-mail: scg@wustl.edu

Received: March 17, 2017
Accepted: June 5, 2017
Online Publication Date: July 28, 2017